5. Tanimoto, T., Um, J., Nishida, K. & Kobayashi, N. Earth's continuous oscillations observed on seismically quiet days. *Geophys. Res. Lett.* **25,** 1553–1556 (1998).

6. Goldreich, P. & Kumar, P. The interaction of acoustic radiation with turbulence. *Astrophys. J.* **326,** 462–478 (1988).

7. Sagan, C. Structure of the lower atmosphere of Venus. *Icarus* **1,** 151–169 (1962).

8. Howard, J. N., Burch, D. E. & Williams, D. Infrared transmission of synthetic atmospheres. Parts I–V. *J. Opt. Soc. Am.* **46,** 186–190, 237–241, 242–245, 334–338, 452–455 (1956).

9. Gilbert, F. Excitation of the normal modes of the Earth by earthquake sources. *Geophys. J. R. Astron. Soc.* **22,** 223–226 (1970).

10. Osaki, Y. in *Progress of Seismology of the Sun and Stars* (eds Osaki, Y. & Shibahashi, H.) 75–86 (Lecture Notes in Physics Vol. 367, Springer, Berlin, 1989).

11. Wielandt, E. & Streckeisen, G. The leafspring seismometer: design and performance. *Bull. Seismol. Soc. Am.* **72,** 2349–2367 (1982).

12. Kamal & Mansinha, L. A test of the superconducting gravimeter as a long-period seismometer. *Phys. Earth Planet. Inter.* **71,** 52–60 (1992).

13. Smith, S. W. IRIS: A program for the next decade. *Eos* **67,** 213–219 (1986).

14. Dziewonski, A. M. & Woodhouse, J. H. An experiment in the systematic study of global seismicity: centroid-moment tensor solutions for 201 moderate and large earthquakes of 1981. *J. Geophys. Res.* **88,** 3247–3271 (1983).

15. Bullen, K. E. & Bolt, B. A. *An Introduction to the Theory of Seismology* 4th edn (Cambridge Univ. Press, 1985).

16. Beroza, G. & Jordan, T. Searching for slow and silent earthquakes using free oscillations. *J. Geophys. Res.* **95,** 2485–2510 (1990).

17. Turcotte, D. L. & Schubert, G. *Geodynamics Applications of Continuum Physics to Geological Problems* (Wiley, New York, 1982).

Global and local measures of the intrinsic Josephson coupling in Tl₂Ba₂CuO₆ as a test of the interlayer tunnelling model

A. A. Tsvetkov*†, D. van der Marel*, K. A. Moler‡,
J. R. Kirtley§, J. L. de Boer*, A. Meetsma*, Z. F. Ren∥,
N. Koleshnikov¶, D. Dulic*, A. Damascelli*, M. Grüninger*,
J. Schützmann*, J. W. van der Eb*, H. S. Somal* & J. H. Wang∥

* *Materials Science Centre, University of Groningen, 9747 AG Groningen, The Netherlands*
† *P. N. Lebedev Physical Institute, 117924 Moscow, Russia*
‡ *Department of Physics, Princeton University, Princeton, New Jersey 08544, USA*
§ *IBM T. J. Watson Research Center, PO Box 218, Yorktown Heights, New York 10598, USA*
∥ *Department of Chemistry, SUNY at Buffalo, Buffalo, New York 14260-3000, USA*
¶ *Institute of Solid State Physics, Russian Academy of Sciences, Chernogolovka, Russia*

....

One leading candidate theory of high-temperature superconductivity in the copper oxide systems is the interlayer tunnelling (ILT) mechanism[1]. In this model, superconductivity is created by tunnelling of electron pairs between the copper oxide planes—contrasting with other models in which superconductivity first arises by electron pairing within each plane. The ILT model predicts that the superconducting condensation energy is approximately equal to the gain in kinetic energy of the electron pairs due to tunnelling. Both these energies can be determined independently[2–4], providing a quantitative test of the model. The gain in kinetic energy of the electron pairs is related to the interlayer plasma frequency, ω_J, of electron pair oscillations, which can be measured using infrared spectroscopy. Direct imaging of magnetic flux vortices also provides a test[5], which is performed here on the same samples. In the high-temperature superconductor Tl₂Ba₂CuO₆, both the sample-averaging optical probe and the local vortex imaging give a consistent value of $\omega_J \approx 28\,\mathrm{cm}^{-1}$ which, when combined with the condensation

energy, produces a discrepancy of at least an order of magnitude with deductions based on the ILT model.

In the ILT model, the normal state is different in nature from the traditional Landau Fermi liquid. As a result, coherent transport of single charge carriers between the planes is strongly inhibited in the normal state. In the superconducting phase, tunnelling of pairs is possible, and the superconducting condensation energy (E_{cond}) in the ILT model is the gain in kinetic energy (E_J) due to the tunnelling of those pairs: $E_{cond} = \eta E_J$. The number η is of the order of 1 when ILT is the only active pairing mechanism[3]. With conventional mechanisms, although usually $\eta \ll 1$, there is no prediction for η that is free from materials parameters. A crucial point in this discussion is that both E_{cond} and E_J are experimentally accessible quantities, thus allowing the experimental verification of the ILT hypothesis. E_{cond} can be measured from the specific heat[6]; E_J can be determined by measuring the interlayer (Josephson) plasma frequency[7].

For this work, we used two kinds of samples: single crystals and epitaxial thin films of Tl₂Ba₂CuO₆. The crystals have a superconducting transition temperature (T_c) of 82 K and transition width (10%–90%) of 13 K, as determined by bulk susceptibility measurements using a superconducting quantum interference device (SQUID). Using 4-circle X-ray diffraction, we verified that the material belongs to the tetragonal I4/*mmm* space group, with (for the crystals) lattice parameters $a = b = 3.867$ Å, and $c = 23.223$ Å. The films have $T_c = 80$ K as determined by d.c. resistivity, and $c = 23.14$ Å. Both types of samples have relatively large physical dimensions perpendicular to the c-axis, corresponding to the conducting copper oxide planes (50 mm² for the thin films, and 1 mm² for the crystals). They have small dimensions along the c-axis (∼1 μm for the thin films, and ∼50 μm for the crystals).

To determine the plasma resonance, we measure the reflection coefficient of infrared radiation incident on the a−b-plane at a large angle (80°) with the surface normal[8]. A sketch of our experiments is shown in Fig. 1. In the case of the single crystals, the intensity of the reflected light drops below our detection limit if the wavelength exceeds 0.2 mm (that is, for $\omega/2\pi c < 50\,\mathrm{cm}^{-1}$, where ω is an angular frequency and c is the speed of light) due to diffraction. Using thin films we were able to extend this range to 20 cm⁻¹. The electric field vector of the radiation is chosen to be parallel to the plane of incidence, resulting in a large component perpendicular to the CuO₂ planes. This geometry allows absorption of the light by lattice vibrations and plasma-oscillations polarized perpendicular to the planes.
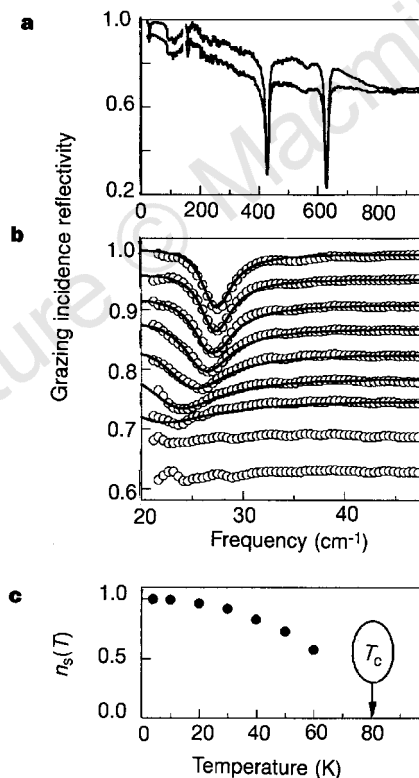
In Fig. 2a we show the single-crystal and thin-film reflectivity for $\omega/2\pi c$ above and below 150 cm⁻¹, respectively. All prominent absorption lines for frequencies above 50 cm⁻¹ correspond to infrared-active lattice vibrations, which show no strong temperature dependence. In the 4 K spectrum we observe a clear absorption
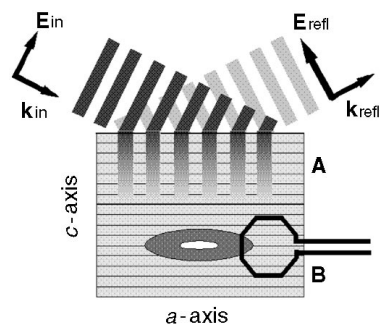
Figure 1 Diagram of the experimental set-up. **A**, Grazing-incidence reflectivity. The p-polarized light incident at a grazing angle sets up a periodic electric field pattern, which is polarized perpendicular to the sample surface, and decays exponentially inside the solid. **B**, Scanning SQUID microscopy. The octagonal pick-up loop detects the magnetic flux perpendicular to the a–c face.

at $\omega_J = 27.8 \, cm^{-1}$. This resonance exhibits a strong red shift on raising the temperature, as shown in Fig. 2b. Above 70 K, it has shifted outside our spectral window. In Fig. 2c we also present the temperature dependence of the resonance position, $\omega_J(T)$, squared and normalized to 4 K, $\omega_J(T)^2/\omega_J(4\,K)^2$. This temperature dependence extrapolates to zero at T_c, which indicates that it is a plasma resonance of the paired charge carriers. We therefore attribute this absorption to a Josephson plasmon, a collective oscillation of the paired charge carriers perpendicular to the coupled superconducting planes[7]. For a purely electronic system the Josephson resonance frequency, c/λ_c, where λ_c is the c-axis penetration depth, is determined by the supercurrent density along the c-axis. Because in the present case the Josephson plasma resonance is located at a frequency below the infrared-active lattice vibrations, the corresponding dynamical electric field is screened by the ions and the lattice vibrations, characterized by a dielectric constant ϵ_{cs}. As a result we observe the Josephson resonance at a reduced frequency $\omega_J = \epsilon_{cs}^{-1/2} c/\lambda_c$. We performed a full optical analysis of these spectra in the spectral range $20-6,000 \, cm^{-1}$ using Fresnel's equations for reflection at an oblique angle of incidence of anisotropic optical media. This way we were able to extract the dielectric function ϵ_{cs} from our data. For frequencies below $40 \, cm^{-1}$, $\epsilon_{cs} = 11.3 \pm 0.5$. We therefore obtain $\lambda_c(4\,K) = 17.0 \pm 0.3 \, \mu m$.

An independent experimental measure of the interlayer coupling is provided by a direct measurement of λ_c. Here we employ the fact that vortices which are orientated parallel to the planes, called interlayer Josephson vortices, have a characteristic size λ_c along the
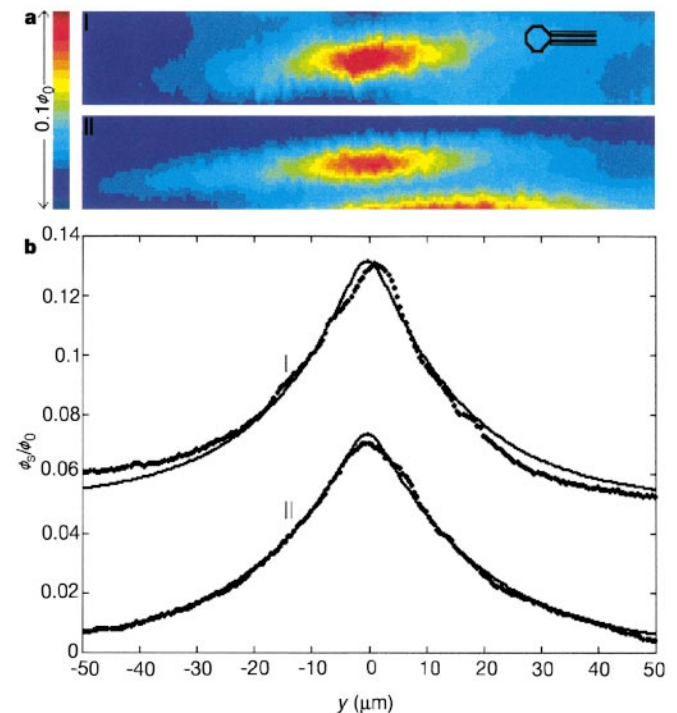
planes and λ_a perpendicular to the planes[9]. In order to determine λ_c directly, we used a scanning SQUID microscope[10] to map the magnetic fields perpendicular to an $a-c$ face at 4 K (Fig. 1B)[5]. The crystal was cooled in a magnetically shielded cryostat with a residual magnetic field of a few milligauss, resulting in the presence of a few isolated trapped vortices (Fig. 3a). The jitter apparent in this image is due to the mechanical scanning mechanism used in our SQUID microscope. With an octagonal pick-up loop of diameter $L = 4 \, \mu m$, the vortices were resolution-limited along the c direction ($\lambda_c \ll L$), but not along the a direction ($\lambda_c > L$).

Fitting the longitudinal cross-sections (Fig. 3b) to the functional form for the magnetic fields of an interlayer Josephson vortex[9] convoluted with the shape of the pick-up loop[5,10] gave the results $\lambda_c = 17 \pm 4 \, \mu m$ and $\lambda_c = 19 \pm 1 \, \mu m$ for these two vortices. The statistical error bars were determined using a criterion of doubling of the variance from the least-squares value, but systematic errors from the background and the shape of the pick-up loop, and the effect of the surface on the shape of the vortex, may be as large as 30%. Using this technique, we imaged vortices in three pieces cut from a large single crystal, which was part of the mosaic used to make the measurements in Fig. 1A. The vortices in all three pieces confirm the plasma resonance frequency of ~28 cm^{-1}. This agreement rules out alternative interpretations of our results[11].

We are now ready to determine E_J using the relation[7] between ω_J and E_J $\omega_{cs}\hbar^2\omega_J^2 = 4\pi d a^{-2} e^{*2} E_J$, where d is the distance between planes (11.6 Å), a is the cell parameter (3.87 Å), $\hbar$ is the Planck constant, and $e^* = 2e$ is the charge of the pairs. The result is

Figure 2 Optical measurements. **a** P-polarized reflectivity at 80° angle of incidence of $Tl_2Ba_2CuO_6$ ($T_c = 82\,K$) at 4 K (upper curve) and 100 K (lower curve). Frequencies above (below) $150 \, cm^{-1}$ correspond to single-crystal (thin-film) data. **b**, Thin-film spectra on an expanded frequency scale. From top to bottom: 4 K, 10 K, 20 K, 30 K, 40 K, 50 K, 60 K, 75 K and 90 K. The curves have been given incremental 3% vertical offsets for clarity. The solid curves correspond to calculations as described in the text. **c**, Temperature dependence of the superfluid density $n_s(T) = \omega_J(T)^2/\omega_J(4\,K)^2$, demonstrating that the resonance frequency converges to zero at T_c.

Figure 3 Local magnetic measurements with a scanning SQUID. **a**, Images of the magnetic field perpendicular to an $a-c$ face of a $Tl_2Ba_2CuO_6$ single crystal in two different locations, showing two different interlayer Josephson vortices. The dashed lines indicate the longitudinal cross-sections. Inset: sketch of the 4-μm octagonal pick-up loop. **b**, The flux through the SQUID pick-up loop along the longitudinal cross-sections. ϕ_S is the magnetic flux through the SQUID pick-up loop; $\phi_0 = 20.7 \, G \, \mu m^2$ is the superconducting flux quantum. The solid curves are fits which determine the c-axis penetration depths of these two vortices to be (I) $\lambda_c = 17 \pm 4 \, \mu m$ and (II) $\lambda_c = 19 \pm 1 \, \mu m$.

$E_J = 0.24 \, \mu eV$ per formula unit. For $Tl_2Ba_2CuO_6$, the measured value of E_{cond} is $100 \pm 20 \, \mu eV$ per formula unit[6]. Hence $\eta = E_J/E_{cond} = 0.0024 \pm 0.0005$, which is clearly at variance with the notion that condensation in the high-T_c superconductors is due to the gain in kinetic energy of the pairs (E_J) in the superconducting state. □

1. Anderson, P. W. *The Theory of Superconductivity in the High-T_c Cuprates* (Princeton Univ. Press, 1997).
2. Anderson, P. W. Interlayer tunnelling mechanism for high-T_c superconductivity: comparison with c axis infrared experiments. *Science* **268,** 1154–1155 (1995).
3. Leggett, A. J. Interlayer tunnelling models: implications of a recent experiment. *Science* **274,** 587–590 (1996).
4. van der Marel, D., Schützmann, J., Somal, H. S. & van der Eb, J. W. in *Proc. 10th Anniversary HTS Workshop on Physics, Materials & Applications* (eds Batlogg, B., Chu, C. W., Chu, W. K., Gubser, D. U. & Müller, K. A.) 357–370 (World Scientific, Rivers Edge, NJ, 1996).
5. Moler, k. A., Kirtley, J. R., Hinks, D. G., Li, T. W. & Xu, M. Images of interlayer Josephson vortices in $Tl_2Ba_2CuO_{6+\delta}$. *Science* **279,** 1193–1195 (1998).
6. Loram, J., Mirza, K. A., Wade, J. M., Cooper, J. R. & Liang, W. Y. The electronic specific heat of cuprate superconductors. *Physica C* **235,** 134–137 (1994).
7. Lawrence, W. E. & Doniach, S. in *Proc. 12th Int. Conf. on Low Temperature Physics* (ed. Kanda, E.) 361–362 (Academy, Kyoto, 1971).
8. Schützmann, J. *et al.* Experimental test of the inter-layer pairing models for high-Tc superconductivity using grazing incidence infrared reflectometry. *Phys. Rev. B* **55,** 11118–11121 (1997).
9. Clem, J. R. & Coffey, M. W. Viscous flux motion in a Josephson-coupled layer model of high-T_c superconductors. *Phys. Rev. B* **42,** 6209–6216 (1990).
10. Kirtley, J. R. *et al.* High-resolution scanning SQUID microscope. *Appl. Phys. Lett.* **66,** 1138–1140 (1995).
11. Anderson, P. W. c-Axis electrodynamics as evidence for the interlayer theory of high-temperature superconductivity. *Science* **279,** 1196–1197 (1998).

Ultra-low-threshold field emission from conjugated polymers

I. Musa, D. A. I. Munindrasdasa, G. A. J. Amaratunga & W. Eccleston

Department of Electrical Engineering and Electronics, University of Liverpool, Liverpool L693BX, UK

Field-emission displays contain materials that emit electrons when charged to a low (negative) potential; the electrons excite light emission from phosphor screens. These devices have the potential to provide flat-panel visual displays with good picture quality at low power consumption and low cost[1]. Field-emission devices at present use arrays of microfabricated tips as the emitting cathodes, but a potentially cheaper and simpler alternative is to use a thin-film cathode. This requires the identification of materials that will emit an appreciable electron current at low applied fields. Nitrogen-doped, chemical-vapour-deposited diamond films[2] and amorphous carbon films[3] have been explored for this purpose. The low electron affinity[4], wide bandgap and excellent transport properties[5] of some conducting organic polymers suggest that they might also provide good cathode materials. Here we demonstrate that this is so, reporting field emission from thin films of regioregular poly(3-octylthiophene) deposited on n-doped silicon, with indium tin oxide as the anode. The threshold fields that we measure for electron emission from these films are the lowest yet reported for any carbon-based material.

Regioregular poly(3-octylthiophene) (P3OT) pellets were synthesized by the technique reported by Chen *et al.*[6]. Dissolving 5 mg of P3OT in 1 ml of chloroform formed films of thickness 5 μm.

The solution was then cast onto a pre-cleaned $1 \, cm \times 1 \, cm$ highly doped n-Si substrates (resistivity $\approx 0.003-0.01 \, \Omega \, cm$) in a clean non-vacuum atmosphere. The optical Tauc bandgap was determined, at room temperature, to be ~1.75 eV by ultraviolet-visible spectrophotometry (this bandgap is defined as the intercept of the gradient of a $(\alpha E)^{1/2}$ versus E plot with the E axis, where α is absorption coefficient and E the photon energy). This estimate agrees well with those reported elsewhere[6]. In addition, a single broad absorption maximum was observed at ~2.38 eV, which suggests that these 'as synthesized' films are only slightly doped. Nuclear magnetic resonance measurements indicate a regular 'head–tail' arrangement of the alkyl side chains (which can be thought of as a measure of how ordered the polymers are) of >90%. Following casting the $P3OT/n^{++}$-Si devices were immediately placed in a vacuum of pressure $\sim 10^{-7}$ torr to dry for 24 hours.

The field-emission experiments were carried out in the flat plate configuration with an indium tin oxide coated glass anode. The separation between the anode and cathode was varied between $27 \, \mu m$ and $130 \, \mu m$ using glass-fibre spacers. The pressure in the vacuum was $\sim 2 \times 10^{-7}$ torr. Figure 1 shows typical current–voltage ($I-V$) characteristics. Two regions are clearly identified (called here **1** and **2**). Region **1a** and **1b** denotes the emission before 'conditioning', and region **2** is after 'conditioning'. A highly stable and reproducible current level was maintained thereafter. Here conditioning refers to a little-understood phenomenon related to initial electric-field cycling required for cathodes before they show stable emission. It is thought to be related to field-induced removal of surface adsorbates. In the case of polymers, we also speculate that there are possible chemical excitations taking place at the emission sites during conditioning (see later). In our experiments the conditioning field was always below $10 \, V \, \mu m^{-1}$ in order to avoid any influence of vacuum breakdown phenomena, which can occur at fields above $15 \, V \, \mu m^{-1}$ at the pressure used.

The remarkable current density (J)–electric field (F) characteristics, with threshold field of only $\sim 0.2 \, V \, \mu m^{-1}$ for a current density of $1 \, \mu A \, cm^{-2}$, are shown in Fig. 2a. Figure 2b shows the $J-F$ characteristics as a function of anode–cathode spacing. In addition, a slope of 1.8 of the log I–log V plot indicates that a space-charge-limited current (SCLC) may be limiting the emission process. The measured anode voltage versus gap separation is shown in Fig. 2a inset and indicates a nonlinear relationship. This shows that surface and bulk charge properties may be important to the emission process.

The surface morphology of the film was examined by scanning electron microscopy (SEM) both before and after field emission (Fig. 3a–d). There was no apparent explosive destruction to the film which can be associated with discharge current phenomenon during field emission. We also examined the stability of the emission current over time. The emission characteristic recorded over a 16-hour period of continuous emission is shown in Fig. 4. The initial current drops to 55% of its value in 2 hours, and thereafter remains stable. The sensitivity of the emission to a change in pressure was also examined: the emission current dropped to below 10 pA when the pressure rose to 10^{-3} torr.

The polymer films show void-like features on the surface, of density $\sim 4 \times 10^8 \, cm^{-2}$ and of sizes ranging from a 0.40 μm to few micrometres. These could be sites for preferential emission due to electric field intensification at the edges of the voids. Normally, surface field emission is associated with a tunnelling process at the surface, first proposed by Fowler and Nordheim[7]. The relationship between the current density and electric field will then be given by $J/(\beta V)^2 \propto \exp(-\kappa\phi/\beta V)$, where κ is a constant, ϕ is the barrier height and β is a factor (m^{-1}) which converts the local voltage V to the local electric field (βV); a value of $\beta = 1/d$ where d is the anode–cathode separation, signifies an ideal flat surface.

It is usual to plot $\ln(J/F^2)$ as a function of $1/F$. This type of plot is shown in Fig. 1 inset for region **1b**, before conditioning, where a